JOURNAL OF SOLID STATE CHEMISTRY 107, 303–313 (1993)

Influence of the Preparation Method and Doping on the Magnetic and Electrical Properties of $AgNiO_2$

Y. J. SHIN, J. P. DOUMERC,* P. DORDOR, C. DELMAS, M. POUCHARD, AND P. HAGENMULLER

Laboratoire de Chimie du Solide du CNRS, 351 Cours de la Libération, 33405 Talence Cedex, France

Received September 17, 1992; in revised form February 8, 1993; accepted February 9, 1993

Electrical and magnetic properties of delafossite-type $AgNiO_2$ prepared either from $LiNiO_2$ or from $NaNiO_2$ as the precursors have been compared. The difference of behavior is attributed to the well known deviation from stoichiometry of $LiNiO_2$ and to the presence of some Ni atoms in the Li layers whereas such effects may be neglected in $NaNiO_2$. Magnetic interactions are antiferromagnetic ($J < 0$) in $AgNiO_2$, in contrast to $LiNiO_2$ ($J > 0$). This result is ascribed to the evolution of the covalency of the Ni–O bonds. Transport properties are interpreted in the framework of a semimetal model. A comparative approach of the correlation between structure, chemical bond, and electronic delocalization in delafossite-, α-$NaFeO_2$-, and perovskite-type nickel(III) oxides is proposed.

1. Introduction

Some of the present authors have previously attributed the electrical properties of $AgNiO_2$ to a semimetallic character resulting from a slight overlapping between the σ^*(Ni–O) band and the $4d$ (Ag) levels (*1*). This picture should give rise to two kinds of charge carriers: electrons in the Ni–O layers and holes in the Ag ones. This situation can be expressed chemically by the equilibrium

$$Ag^+ + Ni^{3+} \rightleftarrows \text{“}Ag^{2+}\text{”} + Ni^{2+}, \quad (1)$$

which remains strongly shifted toward the left-hand side.

Actually, $AgNiO_2$ can be prepared only by cation exchange reaction between $AgNO_3$ and an intermediate compound such as $LiNiO_2$ or $NaNiO_2$ because of its poor thermal stability (*1, 2*). Recently we have observed that the electrical and magnetic properties of $AgNiO_2$ strongly depend on the nature of the intermediate compounds. As the proposed band overlap seems to be relatively small, it may be supposed that a small change in chemical composition could modify significantly the physical properties of $AgNiO_2$. Therefore, it is worthwhile to compare samples prepared or doped in different ways in order to shift equilibrium (*1*).

In this paper we discuss the physical properties of two $AgNiO_2$ samples—called I and II—prepared from $NaNiO_2$ and $LiNiO_2$, respectively, and a Cu-doped one (sample III).

2. Experimental Conditions

2.1. Sample Preparation

The intermediate compounds $NaNiO_2$, $LiNiO_2$, and $NaNi_{0.95}Cu_{0.05}O_2$ were prepared by direct solid state reactions according to the following relations:

* To whom correspondence should be addressed.

0022-4596/93 $5.00

$$\tfrac{1}{2}\,Na_2O_2 + NiO \xrightarrow{650°C} NaNiO_2$$

$$\tfrac{1}{2}\,Li_2CO_3 + NiO + \tfrac{1}{4}\,O_2 \xrightarrow{750°C} LiNiO_2 + \tfrac{1}{2}\,CO_2\nearrow$$

$$\tfrac{1}{2}\,Na_2O_2 + 0.95\,NiO + 0.05\,CuO \xrightarrow{650°C} NaNi_{0.95}Cu_{0.05}O_2.$$

Because of the volatility of Na_2O_2, an excess of about 3% was used (*3*). Pelletized mixtures of starting materials were put into gold or alumina boats and heated in an oxygen atmosphere. The reaction products were checked by X-ray diffraction.

The alkali nickelates were used for the following exchange reaction (*1*, *4*), performed in an oxidizing flux of $AgNO_3$ and KNO_3 (about 50 mol% of the latter are added to hinder any decomposition of $AgNO_3$ by increasing the nitrate concentration),

$$AgNO_{3(l)} + AMO_{2(s)} \xrightarrow{KNO_3} AgMO_{2(s)} + ANO_{3(l)},$$

where A = Li or Na and M = Ni or $Ni_{0.95}Cu_{0.05}$. An excess of $AgNO_3$ (about 50%) was used in order to complete the reaction. The starting mixtures were sealed in Pyrex tubes, under a pressure of ca. 10 Pa. The reaction was performed at 300°C for 5 days. Dark grey powders were obtained by leaching out the remaining nitrates in water.

2.2. *Sample Characterizations*

Chemical analysis has been carried out by atomic emission spectroscopy at the Laboratoire Central d'Analyse du CNRS.

EPR measurements have been performed with a Bruker ER 200 tt spectrometer.

Room-temperature powder X-ray diffractograms were obtained with a Philips 1050 diffractometer using a copper anticathode. Lattice constants were determined by a least-squares method from the d-values corrected using silicon as an internal standard (a = 5.4305 Å at 25 °C). The X-ray diffractogram of sample I was also recorded at 77 and 420 K with equipment designed in the laboratory.

Magnetic susceptibility was measured using a Manics DSM8 susceptometer.

Electrical conductivity measurements were performed on pellets (ϕ = 5 mm) using a conventional four-probe method. Thermoelectric power (TEP) data were obtained using equipment described elsewhere (*5*).

TABLE I

CHEMICAL ANALYSIS OF $AgNiO_2$ SAMPLES PREPARED FROM $NaNiO_2$(I) AND $LiNiO_2$(II)

	Weight (%)				
Sample	Ag	Ni	O[a]	Li	Na
I	54.15	29.51	16.12	—	0.22
II	50.88	32.06	16.71	0.355	—
Theor. value	54.32	29.56	16.11	—	—

[a]Estimated by difference.

3. Results

3.1. *Chemical Analysis*

Results of chemical analysis (Table I) show that sample I exhibits a very good $AgNiO_2$ stoichiometric composition with only weak traces of sodium. On the contrary, in sample II, the Ag/Ni ratio is smaller than 1 and the atomic concentration of lithium is about five times larger than that of the sodium in sample I.

Unlike the other samples, an EPR signal is observed for sample II (g = 2.11). It can be attributed either to unreacted $LiNiO_2$ (g = 2.1) (*6*) or to some disorder in the distribution of Ni-atoms as discussed in the next section, whereas in sample I the amount of unreacted $NaNiO_2$ is below the sensitivity threshold of our equipment and therefore most of the sodium found by chemical analysis should be located in the $AgNiO_2$ network[1]. Whatever the distribu-

[1] The impossibility of observing an EPR signal in pure $AgNiO_2$ seems to result from the metallic type conductivity of our sample (*7*).

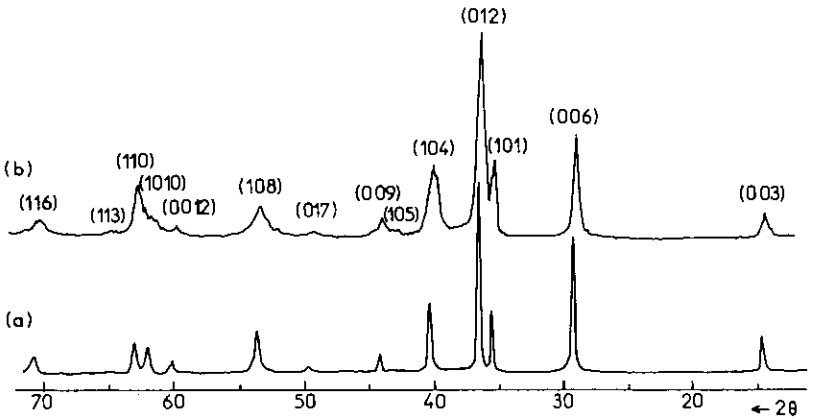

FIG. 1. Powder X-ray diffractograms of sample I (a) and sample II (b) at room temperature.

tion of lithium between the delafossite phase and the $LiNiO_2$-type phase, the lack of silver and the excess of nickel (Table I) suggest the existence of divalent nickel in sample II.

3.2. *X-Ray Characterization*

The X-ray diffractograms of Fig. 1 show that the $AgNiO_2$ samples crystallize with the $3R$-polytype of the delafossite structure (space group $R\bar{3}m$) (*8*). The delafossite-type structure of AMO_2 oxides can be described as a close packing of linear $(AO_2)^{3-}$ groups parallel to the c-axis, the octahedral sites of which are occupied by M^{3+} ions (Fig. 2).

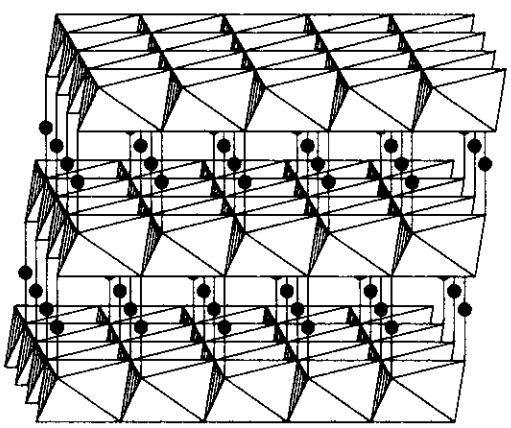

FIG. 2. Delafossite-type structure of AMO_2 oxides. Circles represent A^+ ions located between layers of MO_6 octahedra.

The lattice constants are reported in Table II. No structural change was observed in sample I between 77 and 420 K. Figure 1 shows that, at room temperature, sample II exhibits considerably broader lines than sample I, which can be ascribed to a larger structural disorder. The explanation of this result may be as follows. While in $NaNiO_2$ Na and Ni atoms are well ordered, $LiNiO_2$ always seems to exhibit a weak disorder between Li and Ni atoms. Earlier, Goodenough *et al.* (*9*) pointed out that stoichiometric $LiNiO_2$ is extremely difficult to prepare. A very large atomic exchange between Ni and Li sites has been observed in nonstoichiometric $Li_{1-x}Ni_{1+x}O_2$ prepared at high temperature (*10, 11*). More recently, Goodenough *et al.* reported that $LiNiO_2$ prepared from Li_2CO_3 or LiOH at high tempera-

TABLE II

LATTICE CONSTANTS OF THE HEXAGONAL CELL OF $AgNiO_2$ SAMPLES PREPARED FROM $NaNiO_2$ (SAMPLE I), $LiNiO_2$ (II), AND Cu-DOPED (III)

Sample	a (Å)	c (Å)
I	2.939	18.37
II	2.940	18.35
III	2.939	18.38

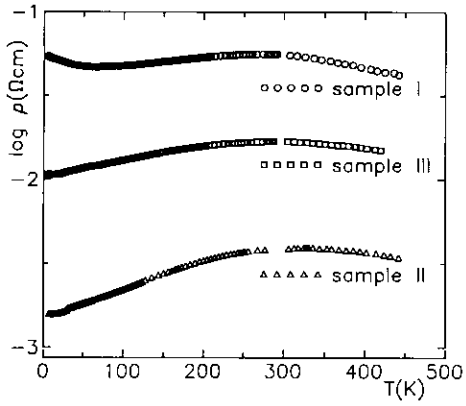

FIG. 3. Thermal variation of the logarithm of the electrical resistivity of $AgNiO_2$ prepared from $NaNiO_2$ (sample I) and $LiNiO_2$ (sample II), and of Cu-doped $AgNiO_2$ (sample III).

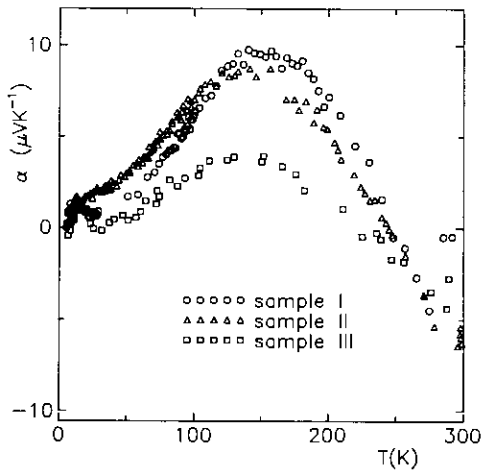

FIG. 4. Thermal variation of the thermopower of $AgNiO_2$ prepared from $NaNiO_2$ (sample I) and $LiNiO_2$ (sample II), and of Cu-doped $AgNiO_2$ (sample III).

ture can be formulated $Li_{1-\delta}Ni_{1+\delta}O_2$ and contains a small number ($\delta = 0.04$–0.08) of Ni atoms located in Li planes (*12*). An excess of nickel has also been detected by Rietveld analysis of X-ray diffractogram (*13*). Therefore, as the exchange reaction is carried out at relatively low temperature, the deviation from stoichiometry and the structural defects of $LiNiO_2$ are expected to play a major part in the chemical composition as well as in the cationic ordering of the resulting delafossite compound.

3.3. Electrical Properties

The thermal variations of electrical resistivity ρ and TEP α of the three samples are given in Figs. 3 and 4. Sample I exhibits larger ρ values than samples II and III. In all samples a change of the sign of the temperature coefficient of resistivity (TCR) $d\rho/dT$ can be detected around 300 K. Sample I undergoes another change of the TCR sign at ~60 K.

In the case of sample I, α exhibits very small positive values below 30 K and then increases up to $+10\ \mu VK^{-1}$ as T increases up to 150 K. For $T > 150$ K, α decreases monotonously and finally becomes negative around 240 K. For sample II, α shows similar behavior, but without such sluggish behavior at low temperature. In sample III, α increases slightly with T until it reaches a value of $+4\ \mu VK^{-1}$ at 135 K, then its sign changes near 230 K.

3.4. Magnetic Properties

Thermal variations of reciprocal magnetic susceptibility corrected for the ion diamag-

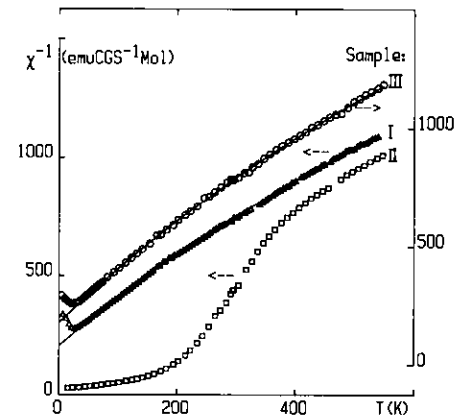

FIG. 5. Thermal variation of the reciprocal molar magnetic susceptibility of $AgNiO_2$ prepared from $NaNiO_2$ (sample I), $LiNiO_2$ (sample II) (above 400 K), and of Cu-doped $AgNiO_2$ (sample III). Solid lines correspond to a Curie–Weiss law (see text and Table III). For sample II, which exhibits a small ferromagnetic component below 400 K (see text), we have plotted M/H with $H = 1.85$ T.

TABLE III

CURIE–WEISS CONSTANTS, TIP AND T_{min} OF $AgNiO_2$ PREPARED FROM $NaNiO_2$ (SAMPLE I), $LiNiO_2$ (II), AND CU-DOPED (III)

Sample	C_M (emuCGSKmol^{-1})	θ_p (K)	TIP (10^{-6} emuCGSmol^{-1})	T_{min} (K)
I	0.460	−105	200	24.5
II($T > 400$ k)	0.650	−95	—	—
III	0.385	−70	230	23

netism (*14*) between 4 and 550 K are plotted in Fig. 5. Samples I and III exhibit a sharp minimum of χ_M^{-1} at a temperature T_{min} equal to 24.5 and 23 K, respectively, suggesting the onset of an antiferromagnetic order at low temperature. The experimental points were fitted with the usual Curie–Weiss law,

$$\chi_M = \frac{C_M}{T - \theta_p} + TIP,$$

and the values of the c_M, θ_p, and TIP parameters are given in Table III.

On the other hand, sample II shows a rather complex behavior. At high temperature ($T > 400$ K), it exhibits a paramagnetic behavior (Table III), whereas a weak ferromagnetic component can be detected below 400 K.

3.5. *Madelung Energy Calculations*

Lattice energies, Madelung constants, and site potentials of $AgNiO_2$, $LiNiO_2$, and $NaNiO_2$ have been calculated with a method based on the Ewald model (*15*). The used structural parameters are given in Table IV. Due to the lack of precise structural data for the rhombohedral form of $NaNiO_2$, an estimated range of oxygen positions was used. Results are summarized in Table V. They show clearly that the delafossite structure exhibits a larger lattice energy and a stronger potential at the Ni site than the rhombohedral α-$NaFeO_2$ one does.

4. Discussion

4.1. *Energy Diagram*

The earlier schematic *MO* energy diagram of the A_2^{-3} sublattice proposed by Rogers *et al.* implies that the Ag delafossite-type compounds should be semiconductors with a bandgap between the $4d$ (Ag) and the $5s$ bands (*17*). Actually the observed metal-like conductivity of $AgNiO_2$ requires a more complex picture requiring consideration of the Ni–O sublattice. The electronic structure of the Ni–O layers involves a σ^*(Ni–O) band splitted by the effective intraatomic repulsion energy U'_{eff} into a fully occupied lower Hubbard band (LHB) and an empty upper Hubbard band (UHB), otherwise a temperature-independent Pauli-type paramagnetism would be expected instead of the Curie–Weiss paramagnetism observed in the present work (Fig. 5). This result and further considerations given in Ref. (*1*) support the semimetal model based on equilibrium (1) (Fig. 6).

4.2. *Magnetic Properties*

Although C_M is larger than the theoretical spin-only value (0.375), Table III clearly shows that Ni^{3+} ions in $AgNiO_2$ have a low-spin configuration ^2E ($t_2^6e^1$) ($S = \frac{1}{2}$). However, unlike $NaNiO_2$ but like $LiNiO_2$, no cooperative Jahn–Teller distortion has been found in $AgNiO_2$ from X-ray diffractograms, at least between 78 and 420 K.

The observed value of TIP (Table III) is much larger than the expected contribution of the Van Vleck term, which may be approximately estimated to 70–80 $\times$ 10^{-6} emuCGS mol^{-1} (*18*). The larger part of this TIP can be attributed to the Pauli-type paramagnetic contribution of the itinerant holes, which, assuming a parabolic band, is given

TABLE IV

CRYSTALLOGRAPHIC PARAMETERS OF $ANiO_2$ (A = Ag, Na, and Li) USED IN MADELUNG ENERGY CALCULATIONS

			$NaNiO_2$[c]	
	$AgNiO_2$[a]	$LiNiO_2$[b]	Monoc. (M)	Rhomb. (R)[d]
Space group	$R\bar{3}m(Z = 3)$	$R\bar{3}m(Z = 3)$	$C2/m(Z = 2)$	$R\bar{3}m(Z = 3)$
Hex. lattice consts. (Å)	$a = 2.939$ $c = 18.37$	$a = 2.882$ $c = 14.20$	$a = 5.33$ $b = 2.86$ $c = 5.59$ $\beta = 110.3°$	$a = 2.96$ $c = 15.77$
A site	(0, 0, 0)	(0, 0, ½)	(0, ½, ½)	(0, 0, ½)
Ni site	(0, 0, ½)	(0, 0, 0)	(0, 0, 0)	(0, 0, 0)
O site	(0, 0, z) $z = 0.1155$	(0, 0, z) $z = 0.2586$	(x, 0, z) $x = 0.278$ $z = 0.795$	(0, 0, z) $z = 0.25$ ($z = 0.26$)
d(A–O) (Å)	2.12 (×2)	2.115 (×6)	2.29 (×4) 2.30 (×2)	2.16 (×6) (2.26 (×6))
d(Ni–O) (Å)	1.94 (×6)	1.974 (X6)	1.95 (×4) 2.17 (×2)	2.16 (×6) (2.06 (×6))

[a]From Rietveld analysis of XRD data; unpublished result.
[b]From Ref. (*13*).
[c]From Ref. (*16*).
[d]The z-value (oxygen) is not known. Two estimated values are proposed.

by the following relationship, taking also into account the diamagnetic orbital contribution (*19*):

$$\chi_{\text{Pauli}} = \frac{4m^*}{h^2}(3\pi^2 n)^{1/3}\mu_B^2\left(1 - \frac{m^2}{3m^{*2}}\right).$$

The TIP value, larger for the Cu-doped than for the undoped materials, suggests an increase of the carrier concentration n. In any case such large values (~200 × 10^{-6} emuCGS mol^{-1}) suggest that the effective mass m^* is enhanced either by electron–electron correlations (*20*) as expected for a low concentration of carriers or by the formation of (small) polarons, or by both effects.

The antiferromagnetic interactions found in the NiO_2 planes of $AgNiO_2$ show a deep contrast with the structurally related compounds $LiNiO_2$ and $NaNiO_2$ which exhibit a ferromagnetic interaction in the NiO_2 sheets with a weak antiferromagnetic coupling between the ferromagnetic layers (*12, 21, 22*). As no direct interaction can be expected between fully occupied t_2 orbitals, the nature of magnetic interactions must be determined by the Ni–O–Ni superexchange interaction as pointed out by Goodenough *et al.* (*12*) for $LiNiO_2$. Following their discussion, the correlation and delocalization interactions (*23*) through e_g-σ_p-σ_p,-e_g overcome the competing t_{2g}-p-e_g delocalization coupling in Ni planes of $LiNiO_2$ and $NaNiO_2$, resulting in the observed ferromagnetic behavior. Conversely, in $AgNiO_2$ the latter coupling should prevail over the former ones, for it is the only possible interaction leading to antiferromagnetic coupling apart from the e_g-σ_s-e_g correlation, whose contribution is usually neglected, as σ_s yields less covalent bonding than σ_p orbitals.

The above conclusion could result from a charge transfer gap ($Ni^{3+} + O^{2-} \rightarrow Ni^{2+} + O^-$) larger for $AgNiO_2$ than for

TABLE V

CALCULATED MADELUNG ENERGIES AND SITE POTENTIALS IN $ANiO_2$ (A = Ag, Na, Li) USING STRUCTURAL DATA OF TABLE IV

	$AgNiO_2$	$LiNiO_2$	$NaNiO_2$ (M)	$NaNiO_2$ (R)[a]
Site-Potential (V)				
A	−9.517	−21.376	−15.416	−21.16 (−18.26)
Ni	−37.145	−26.194	−31.559	−21.43 (−24.50)
O	24.173	21.543	29.092	16.39 (17.57)
Madelung constant	22.228	18.641	41.95	15.54 (16.67)
Madelung energy (eV)	−108.92	−93.156	−113.35	−75.61 (−81.12)

[a]Each value corresponds to a different hypothesis about the oxygen position; see Table IV.

$LiNiO_2$ and/or a correlation gap U'_{eff} ($2Ni^{3+} \rightarrow Ni^{2+} + Ni^{4+}$) smaller for $AgNiO_2$ than for $LiNiO_2$. The former effect may be explained by a Ni–O bond more ionic in $AgNiO_2$ than in $LiNiO_2$ which indeed could be expected if we remember that a strongly covalent Ag–O bond competes with the Ni–O bond in the Ag-delafossite. Three additional effects may contribute to a large charge transfer gap in Ag-delafossite. One of them is the large absolute value of the negative Madelung potential (Table V) at the Ni-site, but two others can account for a large stabilization of the O:2p levels in $AgNiO_2$: (*i*) the large value of the Madelung potential at the oxygen site and (*ii*) the lack of a O:2p_π bond since oxygen atoms experience four σ bonds with four neighboring cations (3 Ni + 1 Ag). This situation, for instance, contrasts with that of $LnNiO_3$ (Ln = La, Pr, Nd, Sm, and Ho) perovskites where oxygen atoms are bonded to two nickel atoms by only two σ-bonds involving a sp hybridization, and the other p orbitals lie at a higher energy, giving rise to a small charge transfer gap (*24*).

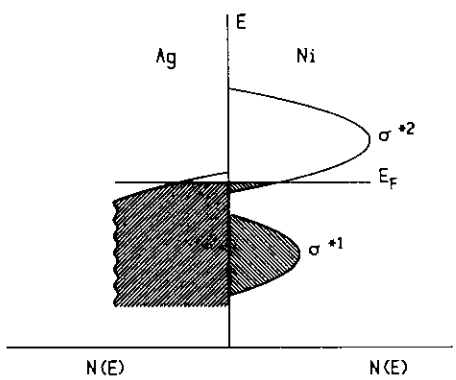

FIG. 6. Schematic energy diagram for $AgNiO_2$ showing the two Hubbard bands and the 4d (Ag) band overlapping the σ^{*2}(Ni–O) upper Hubbard band.

A comparison of the Cu-doped sample (III) with the stoichiometric sample I (Table III) shows that the C_M and θ_p parameters and, to a smaller extent, T_{min} decrease. Such an evolution can be ascribed to the presence of either Cu^{3+} or Cu^{2+} ions within the Ni-planes, which contributes to weakening the exchange integral J as well as to the onset of long range ordering.

At this point we may summarize the arguments in favor of the localization of Cu atoms within the nickel planes rather than the Ag-planes: (i) the decrease of J observed

when doping with Cu, (ii) the tendency of Ni^{3+} to oxidize Cu^{+} into Cu^{2+} which, no more than Cu^{3+}, can occupy a twofold coordinated site, (iii) the up to date impossibility to prepare $Cu^{+}Ni^{3+}O_2$, (*iv*) the increased conductivity (see below) of the Cu-doped sample unexpected at low temperature if Cu atoms were (randomly) distributed in the conducting Ag planes.

An apparently odd evolution of the magnetic properties is observed as the precursor compound is changed from $NaNiO_2$ to $LiNiO_2$. In the latter case (sample II) the ferromagnetic component could be due to either the presence of Ni^{2+} ions located in the Ag planes or the existence of a separate $LiNiO_2$-type phase. It is interesting to note that the curve of sample II in Fig. 5 very well fits a plot corresponding to a mixture of $AgNiO_2$ with 10 mol% of $LiNiO_2$ (using sample I data for $AgNiO_2$ and unpublished data that are in very good agreement with those of (*21*) for $LiNiO_2$).

4.3. Transport Properties

As the present investigation is carried out on polycrystalline samples, the discussion of transport properties is of course confined to some qualitative considerations. On the basis of structural data and previous investigations on various delafossite oxides (*17*) we may assume that electronic transport is easier within the Ag and Ni planes than along the *c*-axis. Therefore, the measured electrical conductivity mainly shows the contribution of the electronic transport ($\sigma_\perp$) perpendicular to the *c*-axis. It should be smaller than the actual value, but we assume that its temperature dependence (as well as that of α) remains meaningful.

Below ca. 240 K, TEP is positive (Fig. 4) showing that carriers are mainly holes. Figure 4 clearly shows that α tends to zero as the temperature tends to 0 K, at least in the limits of experimental accuracy. Such behavior confirms that the number of carriers is not thermally activated as expected for a semimetal.

As ρ tends to a finite value when T tends to 0 K, charge carriers either are itinerant or diffuse with a hopping enthalpy equal to zero, as recently suggested for instance by some authors for strontium-substituted La_2CuO_4 (*25*). Such a transport mechanism should give rise to a linear variation of ρ vs T which is indeed observed between 100 and 200 K (Fig. 7)[2]. In any case we may assume that, between 30 and 150 K where the TEP varies linearly with T, α is given by (*19*):

$$\alpha = \frac{\pi^2 k^2 T}{3e}\left(\frac{d \ln \sigma(E)}{dE}\right) E_F. \qquad (2)$$

In stoichiometric $AgNiO_2$, holes are generated by shifting equilibrium (1) toward the right-hand side, which corresponds to band overlapping in the semimetal picture of Fig. 6. The Cu-doped sample (III) exhibits a smaller $d\alpha/dt$ slope than pure $AgNiO_2$ (sample I). Such a result can be ascribed to a larger hole concentration which is in favor of the formation of Cu^{2+} rather than Cu^{3+} according to the relation

$$Ag^{+} + Cu^{3+} \rightleftarrows \text{“}Ag^{2+}\text{”} + Cu^{2+}.$$

On the other hand, chemical analysis sug-

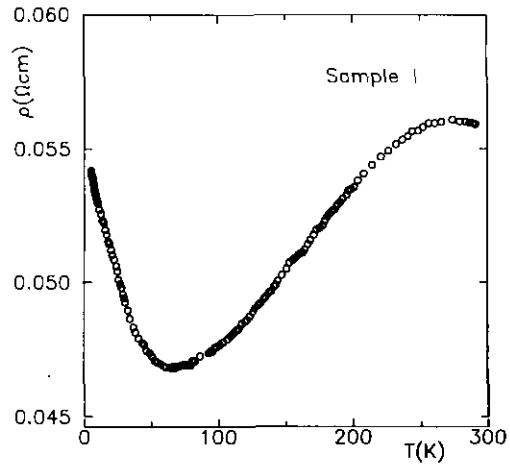

FIG. 7. Thermal variation of the electrical resistivity of pure $AgNiO_2$ (sample I).

[2] Such behavior is also expected for phonon scattering of itinerant carriers in a normal metal above the Debye temperature.

gests that sample II contains Ni^{2+} ions which should shift equilibrium (1) toward the left-hand side (or lift the Fermi level in Fig. 6) and lead to a decrease of the hole density. However, sample II does not exhibit any significant difference in the $d\alpha/dT$ slope with respect to sample I. The apparent discrepancy could result from the structural disorder of sample (II). The disorder must induce a band broadening (*26*) and hence a larger band overlap leading to a change in the density of states and in other parameters involved in the quantity $\sigma(E)$ appearing in Eq. (2). Finally, this effect could compensate the decrease of the hole density.

While the general behavior of our materials is well explained by a semimetal model, two points can be further discussed: (i) the existence of a maximum of resistivity and a change of sign of α at ca. 240 K and (ii) a minimum of resistivity at 60 K in sample I.

As a rule, when holes (h) and electrons (e) can simultaneously carry a current, the conductivity and TEP are given by the usual equations,

$$\sigma = \sigma_h + \sigma_e \tag{3}$$

and

$$\alpha = \frac{\alpha_h\sigma_h + \alpha_e\sigma_e}{\sigma_h + \sigma_e}. \tag{4}$$

The low temperature behavior (60 K $\leq T \leq$ 250 K) shows that σ_h decreases as T increases. If we assume that σ_h continues to vary in the same way near room temperature, the increase of σ above 300 K implies that σ_e increases with T (Eq. (3)). Such behavior can also explain the change of sign of α at 240 K (Eq. (4)). Therefore, either the number[3] or the mobility of electrons in the Ni planes is thermally activated.

[3] This situation could occur for instance if electrons were trapped as localized Ni^{2+} states forming a donor level stabilized below the bottom of the σ^*(Ni–O) UHB. Such a localization could result from the formation of small polarons.

This result suggests that the hole mean free path is small, as could be anticipated from the large resistivity values which not result only from a low carrier density of semimetal type. The presence of Na atoms within the Ag planes in the case of sample I and the structural disorder in the case of sample II may also contribute to a short mean free path.

The electrical resistivity of sample I exhibits a minimum near 60 K (Fig. 7). Such behavior is well known in metallic alloys and metallic glasses containing *d*-elements, but is rather rare in metallic (or insulating) oxides. Howson and Gallagher (*27*) have pointed out that four main effects may account for such a minimum in the ρ vs T curve. The first one is the well known Kondo effect (*28*). We think that if some magnetic Ni^{3+} or Ni^{2+} ions were responsible for a Kondo-type effect it should be larger or at least present in sample II where the amount of Ni atoms in the Ag planes is expected to be larger than in sample I (see Section 3.2). The second effect listed by the above authors is scattering from two-level states but it seems only applicable to glasses and amorphous materials (*27*). The third one is a quantum interference effect. Elastic collision with small relaxation times may give rise to quantum interferences which increase the resistivity at low temperature where they are expected to be the main scattering mechanism (*29*). Quantum interferences are destroyed by inelastic scattering so that, as T increases, phonon scattering leads to decreased resistivity. At high enough temperatures normal inelastic phonon scattering becomes the predominant mechanism and the usual increase of ρ vs T is observed. The fourth effect which can give rise to an increase of σ with T in a metallic system results from long-range electron–electron interactions (*30*). These last two effects are expected to occur near the metal–insulator transition and are predicted to be particularly efficient in 2D systems where the influence of disorder

(even very weak) should lead to electronic localization (*27, 29*). Another origin for a tendency to localization even applicable in an impurity-free or defect-free crystal is the possibility of a strong electron–phonon interaction which can eventually lead to the formation of polarons. Such an electron–phonon mass enhancement could explain the hump in the TEP variation observed at ca. 20 K for sample I (*27*).

5. Conclusion

The present investigation initiated by the strong dependence of the electrical and magnetic properties of $AgNiO_2$ samples on the precursor used for the preparation has confirmed the previous semimetal model involving an overlapping of the σ^*(Ni–O) band with the 4*d* (Ag) band. Comparison of the $AgNiO_2$ delafossite with either $LiNiO_2$ and $NaNiO_2$ of the α-$NaFeO_2$-type structure or with the $LnNiO_3$ (*Ln* = La, Pr, Nd, Sm, and Ho) perovskites shows that the O → Ni charge transfer gap is larger in the former oxide, especially as the O:2*p* levels are more stable. As a consequence the Ni–O bond is more covalent in the perovskite and a (highly correlated) electron gas is observed (at least for *Ln* = La, Nd). In contrast despite a Ni–O distance of the same magnitude (1.94–1.95 Å) as in the perovskite, most of the nickel electrons are localized in $AgNiO_2$. In addition to the more ionic Ni–O bond mentioned above, two other effects may contribute to this behavior: a Ni–O–Ni angle of about 100° instead of about 180° and the 2D character of the structure. This 2D character could also account for the strong influence of impurities on the transport properties.

Acknowledgment

The authors thank J. C. Grenier for helpful discussions and advice especially on magnetic measurements. They are indebted to E. Marquestaut for his technical contribution in electrical measurements. One of them (Y. J. Shin) is grateful for the financial support of Sunkyong Magnetics, Ltd. (Seoul, ROK).

References

1. A. Wichainchai, P. Dordor, J. P. Doumerc, E. Marquestaut, M. Pouchard and P. Hagenmuller, *J. Solid State Chem.* **74,** 126 (1988).
2. P. N. Bitutskii and V. I. Khitrove, *J. Struct. Chem.* **9,** 921 (1968).
3. V. K. Hestermann and R. Hoppe, *Z. Anorg. Allg. Chem.* **367,** 261 (1969).
4. R. D. Shannon, D. B. Rogers, and C. T. Prewitt, *Inorg. Chem.* **10,** 713 (1971).
5. P. Dordor, E. Marquestaut, and G. Villeneuve, *Rev. Phys. Appl.* **15,** 1607 (1980).
6. I. Yamada, K. Ubukoshi, and K. Hirakawa, *J. Phys. Soc. Jpn.* **54,** 3571 (1985).
7. Z. M. Ziman, "Principles of the Theory of Solids," Cambridge University Press, Cambridge (1964).
8. J. P. Doumerc, A. Ammar, A. Wichainchai, M. Pouchard, and P. Hagenmuller, *J. Phys. Chem. Solids* **48,** 37 (1987).
9. J. B. Goodenough, D. G. Wickham, and W. J. Croft, *J. Phys. Chem. Solids* **5,** 107 (1958).
10. H. Taguchi and Y. Takahashi, *J. Mater. Sci.* **19,** 3347 (1984).
11. J. Morales, C. Pérez-Vicente, and J. L. Tirado, *Mater. Res. Bull.* **25,** 623 (1990).
12. G. Dutta, A. Manthiram, J. B. Goodenough, and J.-C. Grenier, *J. Solid State Chem.* **96,** 123 (1992).
13. I. Saadoune, thesis, University of Bordeaux (1992).
14. Landolt and Börnstein, Vol. II, Springer-Verlag, Berlin/Heidelberg/New York (1966).
15. P. P. Ewald, *Ann. Phys.* **64,** 253 (1921); M. P. Tosi, *Solid State Phys.* **16,** 1 (1964).
16. L. D. Dyer, B. S. Borie, Jr., and G. P. Smith, *J. Am. Chem. Soc.* **76,** 1499 (1954).
17. D. B. Rogers, R. D. Shannon, C. T. Prewitt, and J. L. Gillson, *Inorg. Chem.* **10**(4), 723 (1971).
18. B. N. Figgis, "Introduction to Ligand Fields," Interscience, New York/London/Sydney (1961).
19. N. F. Mott and H. Jones, "The Theory of the Properties of Metals and Alloys," Oxford Univ. Press, Oxford (1936).
20. W. F. Brinkman and T. M. Rice, *Phys. Rev. B* **2,** 4302 (1970).
21. K. Hirakawa, H. Kadowaki, and K. Ubukoshi, *J. Phys. Soc. Jpn.* **54,** 3526 (1985).
22. P. F. Bongers and K. Enz, *Solid State Commun.* **4,** 153 (1966).
23. J. B. Goodenough, *Progr. Solid State Chem.* **5,** 145 (1971).
24. J. B. Torrance, P. Lacorro, C. Asavaroengchai, and R. Metzger, *J. Solid State Chem.* **90,** 168 (1991).
25. J. B. Goodenough, J-S. Zhou, and K. Allen, *J. Mater. Chem.* **1,** 715 (1991).
26. P. W. Anderson, *Phys. Rev.* **109,** 1492 (1958).

27. M. A. HOWSON AND B. L. GALLAGHER, *Phys. Rep.* **170,** 265 (1988).
28. N. W. ASHCROFT AND N. D. MERMIN, "Solid State Physics," Holt, Rinehart, and Winston, New York (1976).
29. N. F. MOTT, "Metal-Insulator Transitions," 2nd ed., Taylor & Francis, London/New York/Philadelphia (1991).
30. B. L. ALTSCHULER AND A. G. ARONOV, *Solid State Commun.* **30,** 115 (1979).